Chapter 5

Experiments

5.1 Performance of the Regularized Curvature Flow

In this section we present an extensive comparison of RCF to other PDE-based techniques based on 4 main principles: image quality, convergence to non-trivial images, automatic stabilization of the iterative process and robustness. The former novel protocol of performance assessment points that RCF and the geometric flows [49], [79] achieve a better compromise between quality of the restored image and stabilization of the iterative process than diffusion-like techniques. However, experiments on real images select RCF as the better posed for non-user gated procedures. An application to segmentation of ultrasonic medical images, [25], proves RCF usefulness in real problems.

5.1.1 Establishing a Stopping Criterion

In practical applications stopping the iterative smoothing can be as important as the quality of the restored image. Even if there are not any image-dependant parameters in the continuous formulation, the numeric algorithm may fail to stop without manual intervention. Stabilization achieved using standard numeric techniques ([18], [70]), ensures that the parameters involved in the stopping stage do not depend upon the particular image restoration. Given a generic iterative scheme:

$$u_{t+1} = u_t + \Delta t \cdot speed$$

two different **stop criteria** can be defined to detect its steady-state:

- Criterion A (critA): *Minimum Speed Value Criterion.* Maximum difference between two consecutive images, i_t, i_{t+1}, should be under a given threshold ϵ, that is:

  $$||i_t - i_{t+1}||_\infty = \max |i_t(x,y) - i_{t+1}(x,y)| < \epsilon$$

  We notice the reader that this criterion only holds when the error in the numeric implementation is negligible. By the considerations of the former Section, RCF

supports this criterion in the case of evolving the signed distance map and, to some extend, low noisy binary images. When numerical errors are difficult to estimate a priori, a more sensible criterion is:

- Criterion B (critB): *Constant Speed Value Criterion.* The iterative process should stop when the magnitude of the speed stabilizes. We consider a magnitude is stable in time when its derivative is under a given threshold, ϵ, in a time interval of a given length T. That is, we stop the evolution at the time T_0 such that $||speed_t - speed_{t+1}||_\infty < \epsilon$ for $t \in [T_0, T_0 + T]$. In the discrete version, the length T converts to a given number of iteration steps, it, via the formula:

$$T = it \cdot \Delta t$$

This criterion is frequently used in iterative schemes prone to oscillate around the equilibrium state, such as snakes [12] or minimizing processes. In the particular case of energy minimization or zero finding, the former stop criteria are also applied to the functional value on the current iteration.

For diffusion processes ([60], [72]), the value *speed* is the divergence term of the PDE we are integrating, for the geometric flows [32], [49], [79] it is the curvature term. For RCF, because the evolution seeks a zero of g, we will apply the stopping criteria to the roughness measure. Maximums will be taken over the whole image in the case of diffusion filtering and over a target curve (representative of the image features) in the case of curvature dependent methods.

Two different kinds of experiments are presented:

• Tests on synthetic images with added noise in order to compare RCF to other PDE-based techniques and determine which ones achieve a better compromise between quality of the restored image and stabilization of the iterative process.

• Performance of RCF in real image filtering and applications to shape recovery.

5.1.2 Experiment I. Comparison to other Filtering Techniques

The methods tested are the Perona-Malik Model (PMM) [60], the Anisotropic Diffusion (AD) method [72], the Mean Curvature Flow (MCF) [32], the Min-Max Flow (MMF) [49] and the Stochastic Geometric Flow (STF) [79]. The time step in the Euler scheme chosen is $\Delta t = 0.1$ for diffusion processes and $\Delta t = 0.4$ for curvature flows.

Methodology of Comparison

We consider that assessment of performance should take into account quality of the restored image as well as the criterion used to decide when the method has reached its best restoration. Quality of the restorations will be measured with the standard quantities:

1. Signal to Noise Ratio (SNR):

$$SNR(I_0, I_{ev}) := 10 log_{10} \left(\frac{\sigma^2(I_{ev})}{\sigma^2(I_0 - I_{ev})} \right)$$

where I_0 denotes the original image and I_{ev} the evolution of the noisy image. The higher it is, the more quality the restored image has.

2. Contrast to Noise Ratio (CTN). This quantity measures the edge preserving rate of the method. It is defined as the

   ratio between the difference of means in the interior (μ_{int}) and exterior (μ_{ext}) of the object of interest and the variance in the exterior (σ_{ext}) of the object of interest:

$$CTN(I) := \frac{|\mu_{ext}(I_{ev}) - \mu_{int}(I_{ev}))|}{\sigma_{ext}(I_{ev})}$$

The issues followed to select the best performer are:
- *Contrast preserving capabilities and overall quality in image restorations.*
- *Convergence to non-trivial steady states*
- *Smooth convergence and stabilization of the iterative process*
- *Robustness to high noise and the embedding Image.*

We have chosen a non-convex M-shape and a circle corrupted with a 50% of uniform noise and a gaussian noise of $\sigma = 0.5$. Any shape reconstructions are obtained applying a threshold of value 0.5 to the filtered images.

Step 1: Best Restorations

Figure 5.1 displays results for the M-shape and figure 5.2 for the circle. Best performances (second columns for uniform noise and third for gaussian one) correspond to the images achieving the best SNR. The number of iterations necessary to reach these images is displayed underneath. Shapes recovered (first columns), correspond to uniform noise, for the M-shape, and gaussian noise, for the circle.

The visual quality of the restored images (fig.5.1 and fig.5.2) is similar for all methods. Background artifacts in some images filtered with RCF are common to all geometric flows. Geometric flows are designed to smooth curves rather than images, therefore they are always prone to produce funny patterns in noisy backgrounds. This is not a main inconvenience if the aim of the filtering procedure is to restore a shape, which is the natural application of geometric flows. In fact, all reconstructed shapes have similar quality, matching the original templates. In the case of STF the circle hexagonal-like appearance could be improved by increasing the number of vertices of the final STF state.

We note that the number of iterations needed to achieve optimal restorations varies with noise.

Step 2: Asymptotic Behavior

Evolution of quality measurements in time (fig.5.3-5.5) reflects convergence to non trivial steady states as well as resemblance between original and evolved images. Final states after 3000 time units are overimpressed on the graphics of fig.5.5.

Plots corresponding to techniques that converge to non-trivial steady states (RCF, MMF and, to some extend, STF) asymptotically tend to a positive number (the final image SNR/CTN value). Meanwhile graphics of methods yielding trivial images (AD,

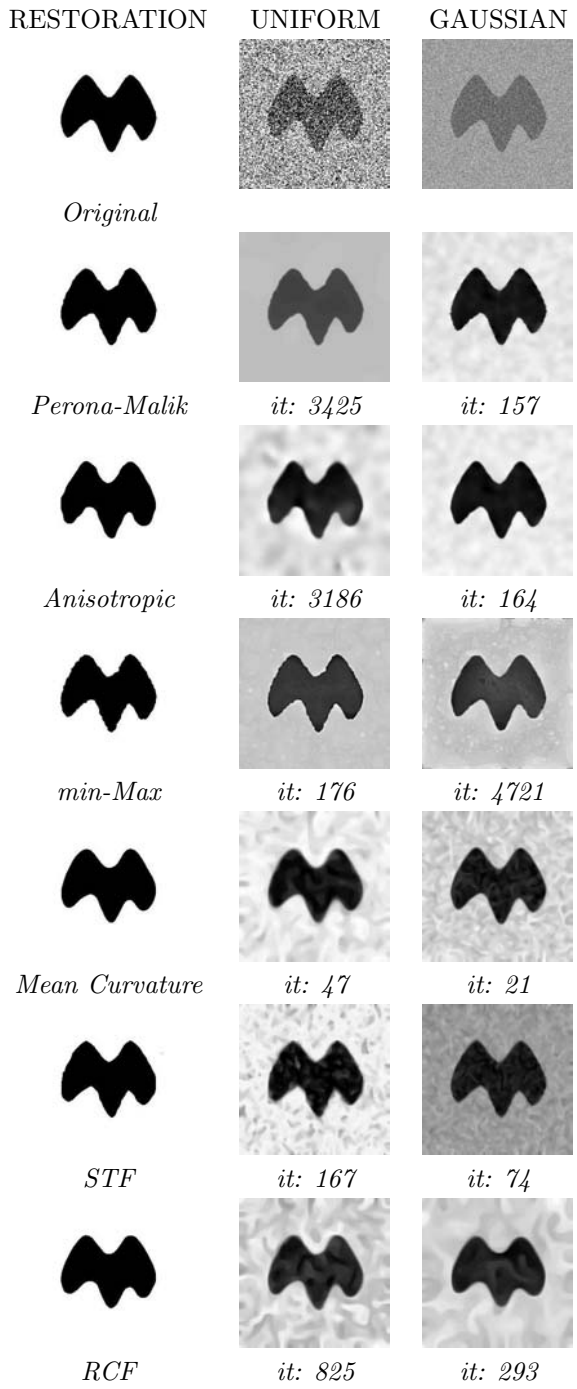

Figure 5.1: M-shape Best Reconstructions.

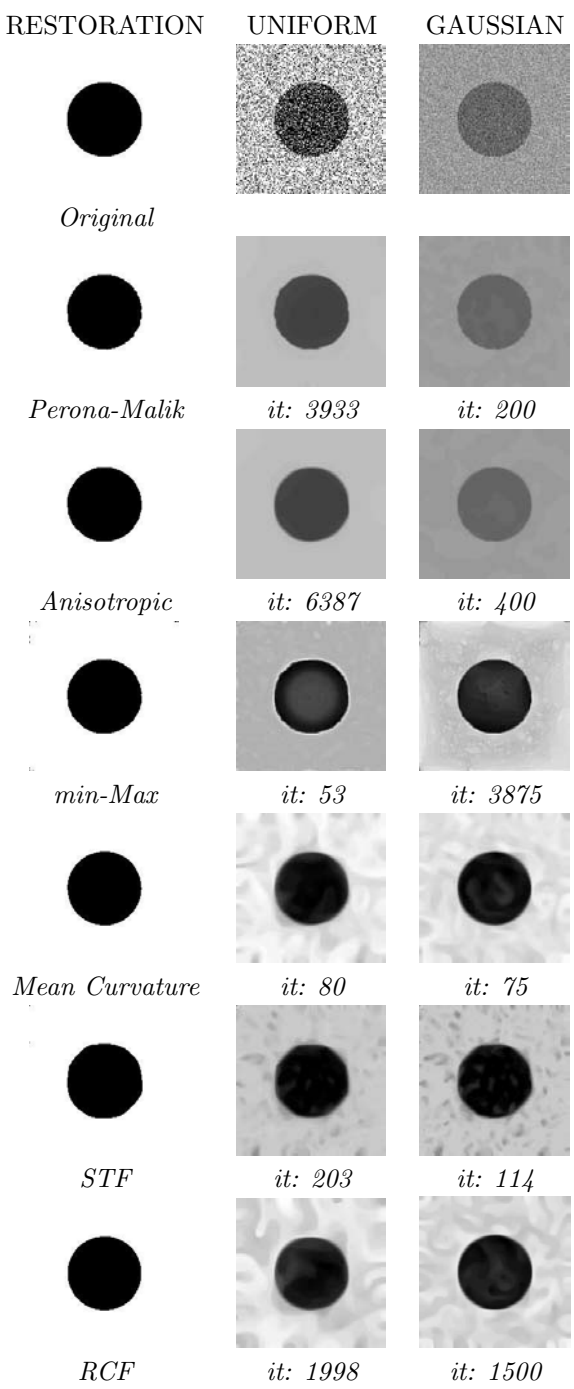

Figure 5.2: Circle Best Reconstructions

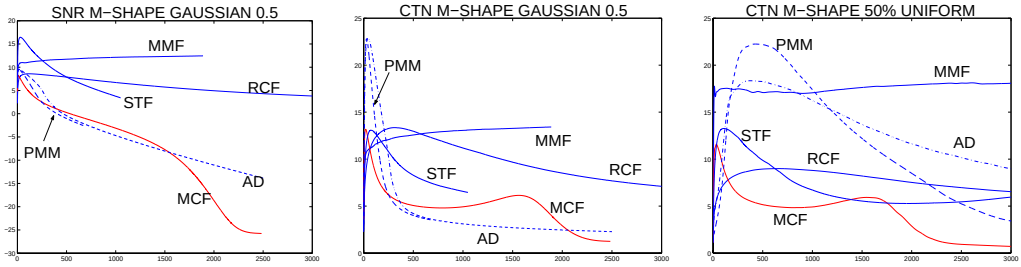

(a) (b) (c)

Figure 5.3: M-Shape Quality Numbers Graphics

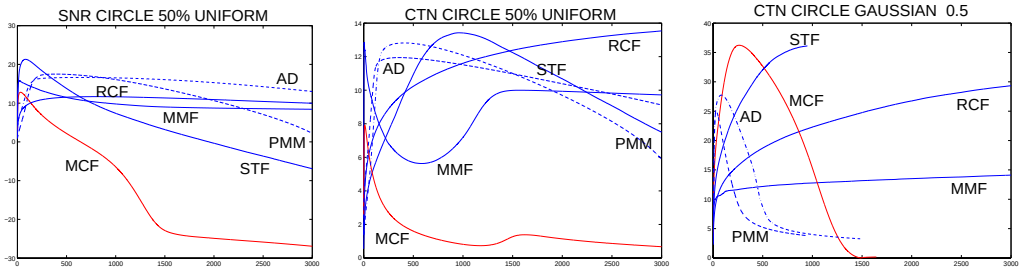

(a) (b) (c)

Figure 5.4: Circle Quality Numbers Graphics

PMM, MCF) present a maximum and then tend to zero at a rate related to the speed of convergence.

Diffusion processes (AD, PMM) fail to maintain quality numbers, especially for CTN values (fig.5.3, 5.4 (b), (c)). The decay is more significant in the measure noise increases and is more prominent in the case of gaussian noise. Geometric flows are more robust against the nature of noise and are more sensitive to the geometry of the underlying shape (see CTN graphics in fig.5.3 (b), (c) and fig.5.4). As expected, MCF is, by no means, the worst performer, especially when non-convex shapes are evolved (fig.5.3, fig.5.5 (a)). Among all techniques, RCF and MMF graphics are the only ones that match, for all cases, the model of a non-trivial steady state. Final images in fig.5.5 reflect quality numbers stability.

Because *Step 2* discards MCF and PMM, *Step 3* will only be applied to AD, MMF, STF and RCF.

Step 3: Evolution Stabilization

The stopping parameters are $\epsilon = 10^{-3}$ for critA and $\{\epsilon = 10^{-4}\ T = 100\}$ for critB. We will keep the former stopping values for the remains of the paper. In order to produce an experiment as balanced as possible, we have tried the criteria on the gaussian noisy M-shape and the uniform noisy circle.

Figures 5.6 and 5.9 plot evolution speeds and RCF roughness measure versus time

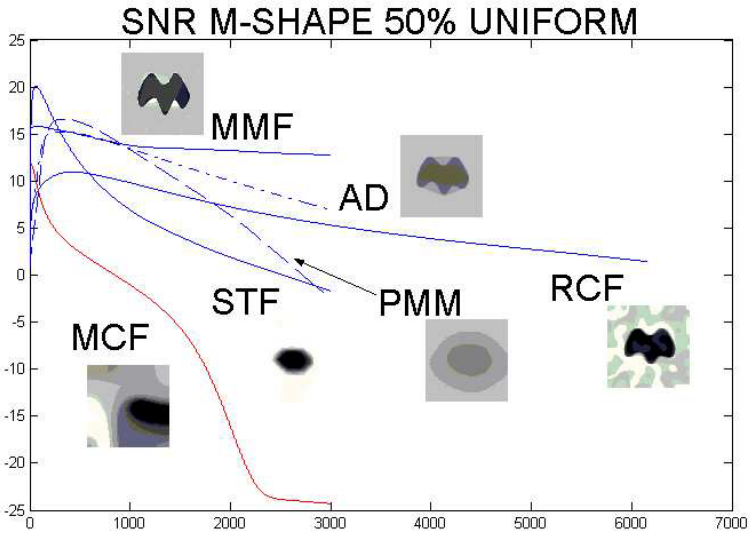

(a)

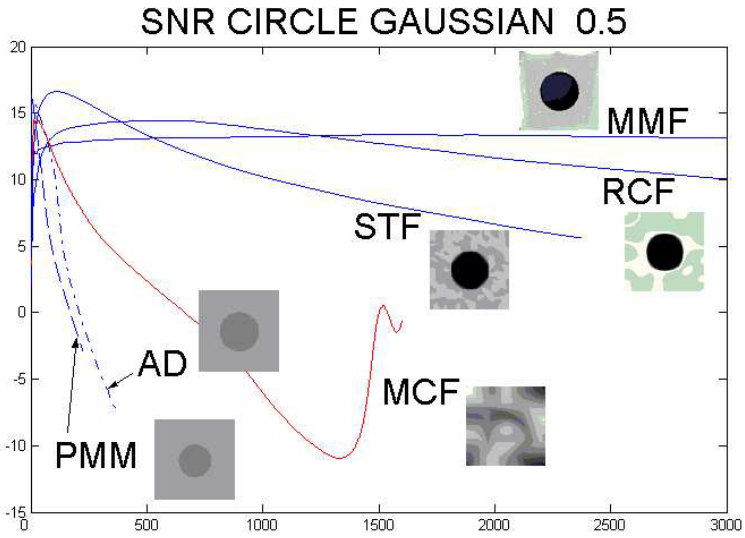

(b)

Figure 5.5: Asymptotic behavior in terms of SNR: (a) uniform noisy M-shape and (b) gaussian noisy circle

in the case of gaussian and uniform noise, respectively. Images stabilized using critA are shown in fig.5.7, 5.10 and those achieved with critB in fig.5.8 and fig.5.11.

Standard numeric stabilization techniques ([18], [70]) need either an accurate implementation (CritA) or a smooth process (CritB). Speed graphics assess their appli-

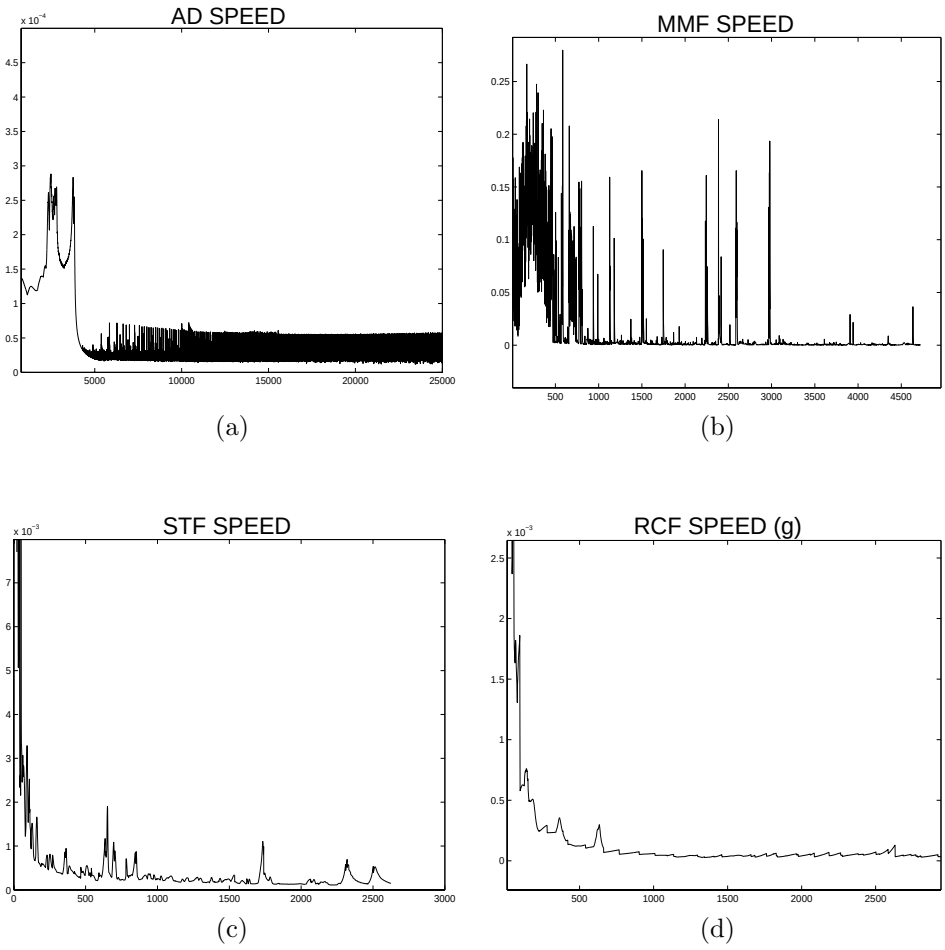

Figure 5.6: Speed Graphics for gaussian noise on the M-shape

cability. If they asymptotically converge to zero, both criteria are valid, CritA is still applicable if plots just tend to zero, while CritB is satisfied for speeds asymptotically converging to a (positive) value. It follows that oscillating or irregular speeds difficult stopping the iterative process.

Both AD and MMF speeds (fig.5.6, fig. 5.9 (a) and (b), respectively) are of an oscillating nature and present a significant lack of smoothness (especially in the case of MMF). This makes critB fail to stabilize the evolution in most cases. Images in fig.5.8 and fig.5.11 (a) correspond to AD final state and fig.5.8 (b) to MMF final state for the gaussian case. Only in the case of uniform noise MMF stabilized using critB (fig.5.9(b)). Regularity of STF speed (fig.5.6 and fig.5.9 (c)) is just on the edge of critB applicability, so that a large time interval T fails to stabilize the evolution. This is a main inconvenience because STF slow noise removal rate makes critB yield images that may not be completely clean (fig.5.8 (c)). On the other side, RCF roughness

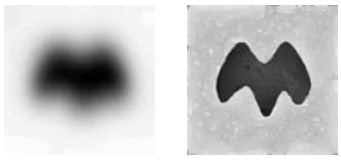

(a) AD (b) MMF

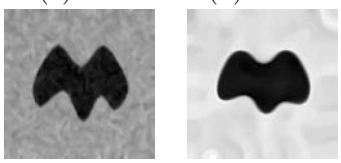

(c) STF (d) RCF

Figure 5.7: Criterion A

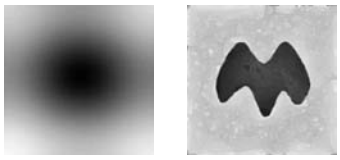

(a) AD (b) MMF

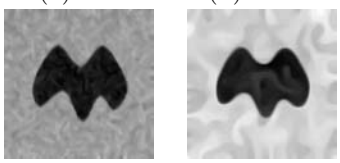

(c) STF (d) RCF

Figure 5.8: Criterion B

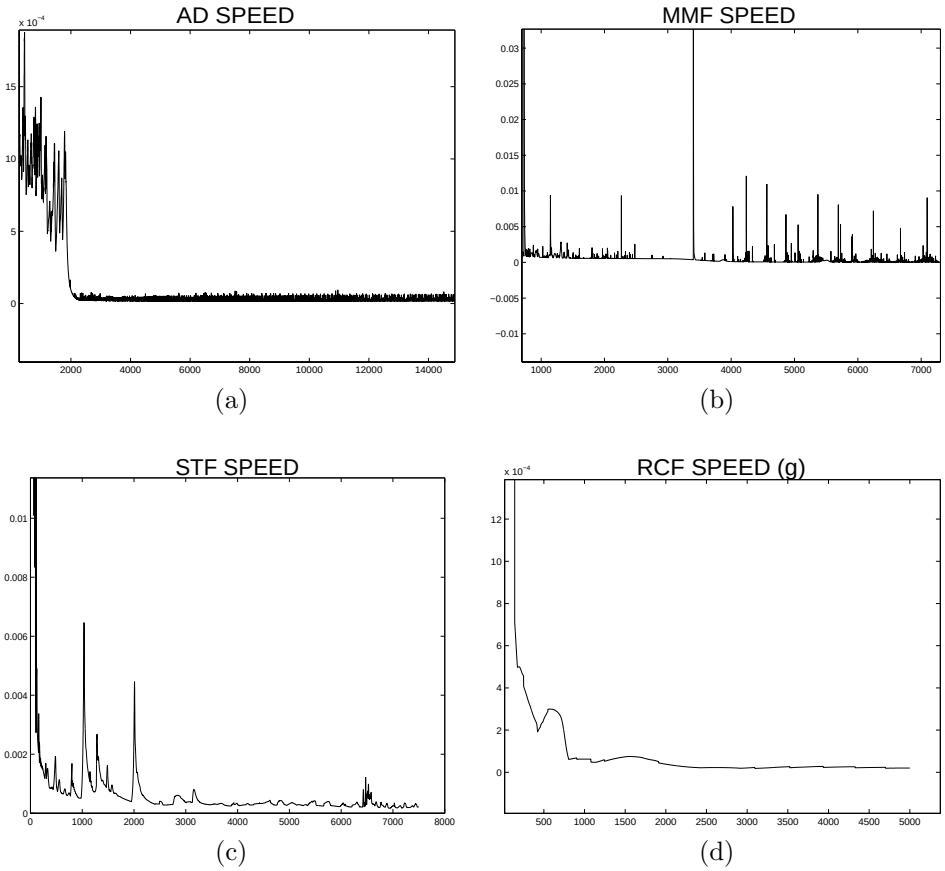

Figure 5.9: Speed Graphics for uniform noise on the circle

measure (fig.5.6 and fig.5.9 (d)) presents a smooth enough asymptotic behavior as to apply critB without strict restrictions. Besides, since RCF is a good noise remover, images in fig.5.8 and fig.5.11 (d) are close to the ones getting best quality numbers in fig.5.1 and fig.5.2.

For all methods, round-off errors in combination with the method behavior difficult success of critA. In the case of AD, rapid convergence to a constant image makes critA stop the evolution at too blurred images (fig.5.7(a)). For MMF, critA reveals to be efficient to stabilize images (fig.5.7, 5.10 (b)), although they may be far from final states because of evolution irregularity. Images obtained with STF present similar anomalies than those achieved with critB. The compromise between noise removal and shape preservation may not be achieved with a fixed ϵ. It follows that the M-shape image (fig.5.7 (c)) still presents background noise, while the circle of the clear image in fig.5.10 (c) starts differing from the theoretical final hexagon that, according to [79], should be the one of maximum size inside the circle. Finally, numeric errors induced by the embedding image may over-erode shapes smoothed with RCF (fig.5.7, 5.10 (d)).

For assessment of quality of the restored shapes in the case of highly noisy images, we will use critA for MMF, STF and critB for RCF.

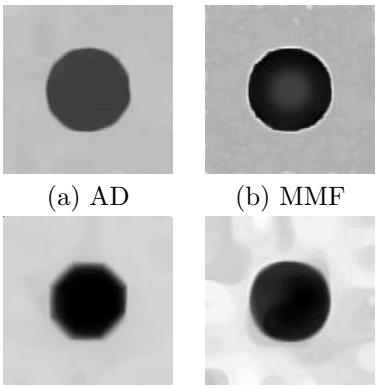

(a) AD (b) MMF

(c) STF (d) RCF

Figure 5.10: Criterion A

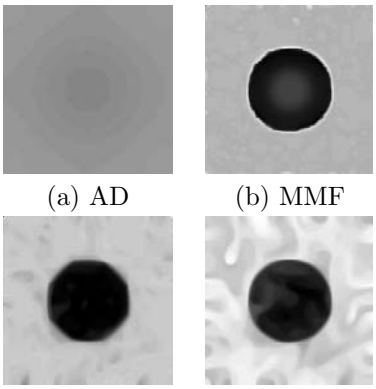

(a) AD (b) MMF

(c) STF (d) RCF

Figure 5.11: Criterion B

Step 4: Robustness

In order to assess robustness, we have corrupted the M-shape with a gaussian noise of parameters $\mu = 0.5$, $\sigma = 1$ (fig.5.12 (a)) and a 70% of uniform noise (fig.5.12 (e)). We have chosen a gaussian noise of positive mean in order to determine the dependence of each of the methods on the gray-level, α_0, defining the curve of interest. We recall that this value is inherent to MMF formulation, as it switches between evolution by negative and positive curvature, while RCF only uses the parameter in its numeric implementation.

Images filtered are in fig.5.12 and the model of shapes restored in fig.5.13. Images filtered with RCF (fig.5.12(d), (h)) are prone to present more background arti-

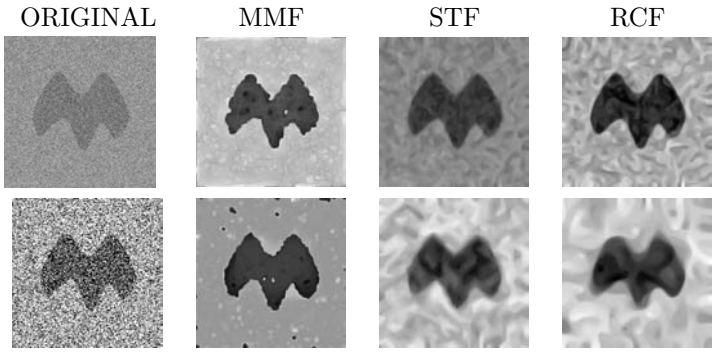

Figure 5.12: Highly noisy M-shape, 1st row gaussian and 2nd uniform

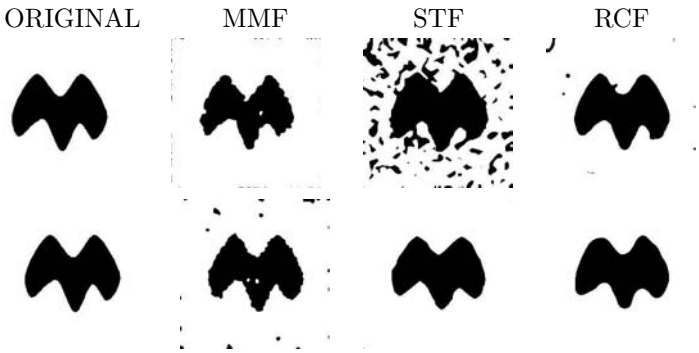

Figure 5.13: Shapes for high noise, 1st row gaussian and 2nd uniform

facts than those that MMF yielded (fig.5.12(b), (f)). However, reconstructed shapes (fig.5.13(d), (h)) are more accurate and smoother for RCF filtered images. Shapes obtained with MMF (fig.5.12(b), (f)) still present irregularities and those obtained with STF may hardly resemble the original ones because of an insufficient noise removed.

The higher irregularity in MMF reconstructions for gaussian noise, reflects its undesirable dependency on the gray-level α_0. In the case of RCF, dependency reduces, in the worst case, into an over erosion of the target shape.

We conclude that not only is our method the one achieving the best compromise between quality of restored image and evolution stabilization, but also the best suited for a non-user intervention application.

5.1.3 Experiment III. Application to Image Filtering and Shape Recovery

This part is devoted to results on real images obtained with RCF and the geometric flows MMF and STF. On one hand, experiments should serve to clarify some of RCF numerical aspects (stopping parameters and speed over target curves). On the other hand they should show those cases where RCF has advantages over MMF and STF.

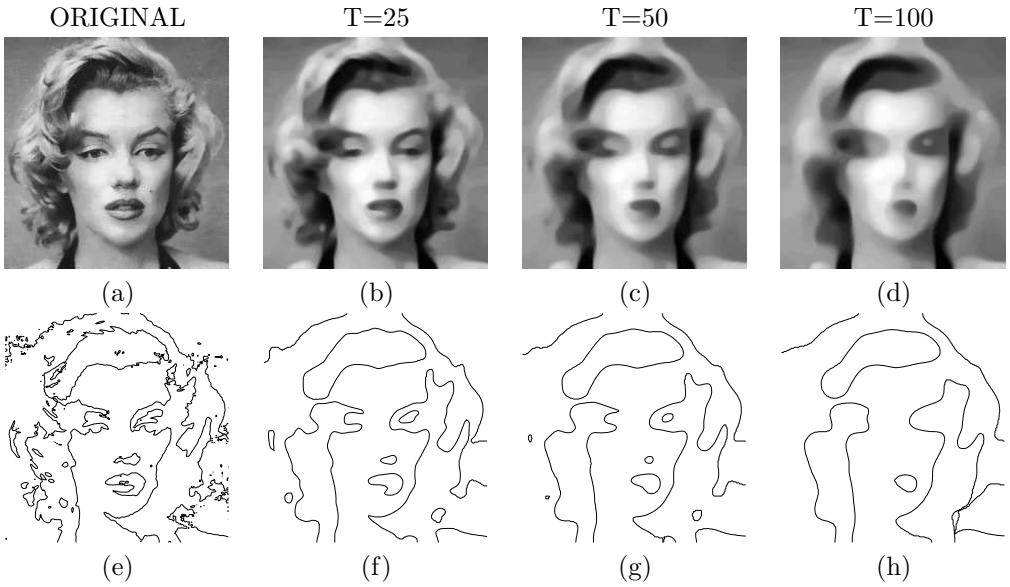

Figure 5.14: Stop parameters impact on RCF filtering of Marilyn, gray-level images are in 1st row and descriptive level set in 2nd one

The following set of real images has been tested:

Faces and Real Objects

The portrait of Marilyn (fig.5.14 (a)) will serve to illustrate the role of T in RCF numeric scheme. We run RCF with $\epsilon = 10^{-3}$ and $T = 25, 50, 100$. Figure 5.14 displays the Marilyn's gray-level images (first row) and the target level curve (second row). Images stabilized with the shortest time intervals (fig.5.14 (b), (c)) keep the most descriptive facial features (eyes, mouth and nose), while spurious details in the hair have been removed (see curves in fig. 5.14 (f), (g)). Besides, although the smoothest Marilyn image (fig.5.14 (d)) may seem rather eroded, the essential facial features are still identified in the target curve (fig.5.14 (h)).

We have chosen the buildings of fig.5.15 (a), (e) for our first comparison between RCF, MMF and STF. Because of their different geometric designs, they will illustrate capability of each of the methods to retain shape models in practical applications. The squared shaped arch of fig.5.15 (a) is perfectly kept by MMF (fig.5.15 (d)) and, though a bit rounder, by RCF (fig.5.15 (b)). Although we used the same parameters than in [79], rectangles have almost disappear in the STF image (fig.5.15 (c)). In the case of fig.5.15 (e), oval arch nicely appears in all filtered images fig.5.15 (f), (g) and (h). Although the ones in RCF image (fig.5.15 (e)) are sharper than in MMF smoothed building (fig.5.15 (g)) and smoother than in STF image (fig.5.15 (f).

Speed plots in fig.5.16 correspond to the building in fig.5.15 (e). Quantities have been computed on the whole image (1st row) and on the level set that best describes the geometry of the building (2nd row). In all three geometric flows, graphics for the

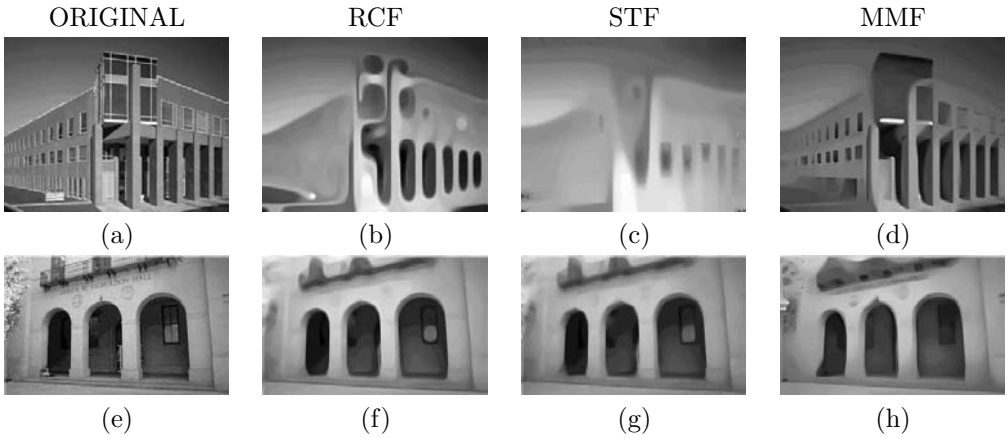

Figure 5.15: Buildings filtering

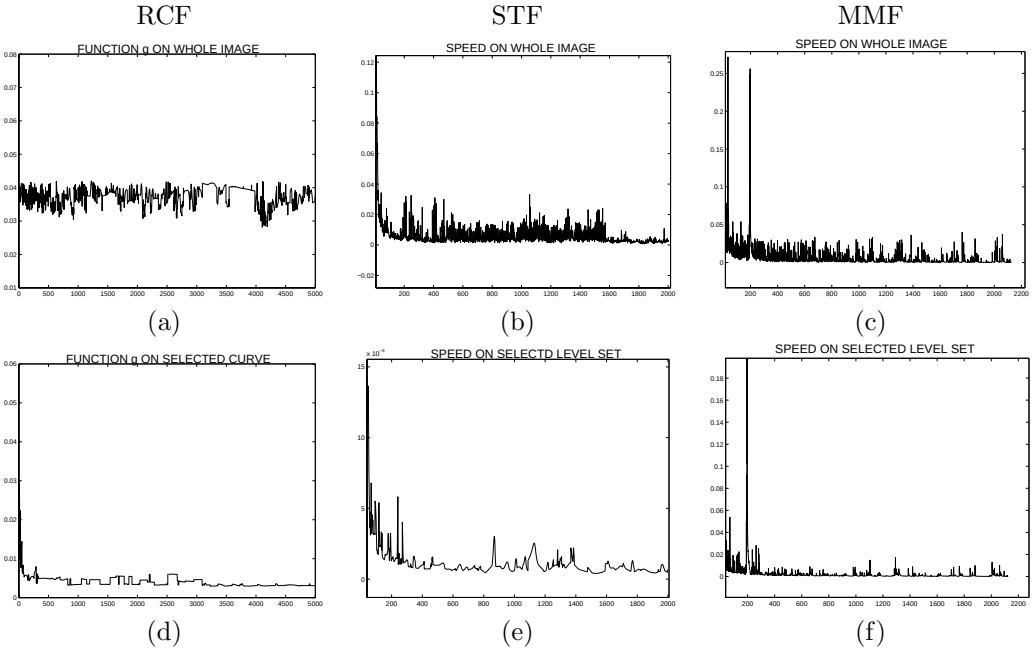

Figure 5.16: Speeds on whole image (1st row) and on selected curve (2nd row) for (a), (d) RCF, (b), (e), STF and (c), (f) MMF

selected curve are smoother in time, which motivates using the latter for evolution stabilization. We note that graphics reflect the error in RCF implementation (Section 2.5): peaks in fig.5.16(d) correspond to the error introduced by the collapsing of a small level curve.

The second comparison on the car plate of fig.5.17(a) shows the contrast preser-

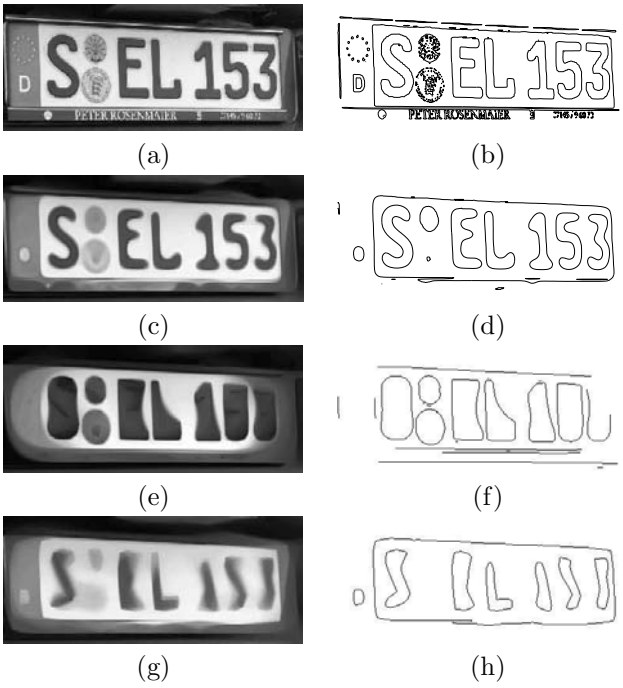

Figure 5.17: Filtering of plate:(a), (b) original, (c), (d), RCF (e), (f) MMF and (g), (h) STF

vation of geometric flows and RCF higher efficiency for shape restoration. Curves in the 2nd column correspond to image canny edges. We argue that the filtering should preserve image sharpness and regularity of the numbers and letters borders (fig.5.17 (b)), while superfluous details (small letters at the plate bottom and stamps) and noise that may mislead a latter segmentation process should be removed. First notice that all three geometric flows stabilize images (fig.5.17 (c), (e) and (f)) with contrast changes equal to the original. Edges (fig.5.17 (d)) of RCF final image yield plate numbers that, though a bit smoother, perfectly match the original ones. Meanwhile, edges extracted from images stabilized with MMF and STF (fig.5.17 (f), (h)) are over-smoothed and the geometry (and even topology) of the resulting numbers is significantly different.

Application to Medical Images

We have applied our technique to segment the luminal area in intravascular ultrasound sequences (IVUS) [25]. Since the grey level of ultrasound images expresses the material impedance, black pixels correspond to blood and white ones to tissue. The aim was to obtain a model of the artery reflecting its geometry by means of a procedure requiring the minimal manual intervention as possible. Artifacts caused by blood flow and the speckled nature of ultrasound images force some kind of smoothing of the level surfaces. RCF has been applied to cross sections and longitudinal cuts using

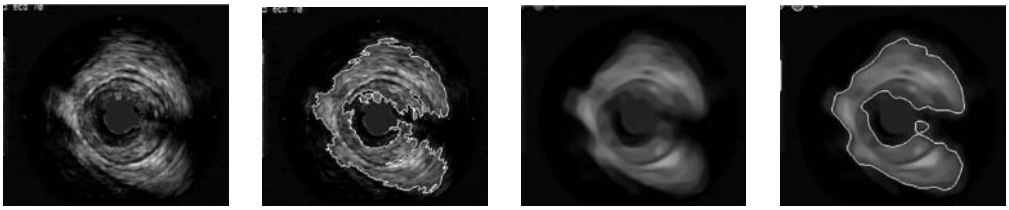

(a) (b) (c) (d)

Figure 5.18: Cross Sections of IVUS sequences. Original IVUS images (a) and segmenting curve (b), steady state attained with RCF (c) and the resulting segmenting curve(d).

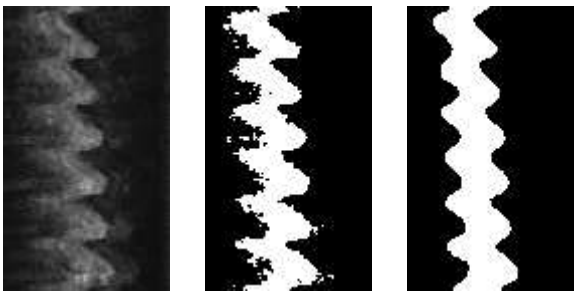

(a) (b) (c)

Figure 5.19: Longitudinal cut of IVUS (a), shape segmenting blood and tissue in (b) the original cut and the smoothed shape with RCF (d).

the speed stabilization criterion over the level curve that best segments blood and tissue.

Figure 5.18(a) shows a cross section of an IVUS sequence and fig.5.18 (b) the level curve that separates blood from tissue. The inner border corresponds to the curve segmenting blood and tissue. The image achieved by RCF is displayed in fig.5.18 (c) and the corresponding segmenting curve in fig.5.18 (d). Notice the way RCF-smoothed curve captures the characteristic features of the curve in fig.5.18 (b), such as the small oval in its inner border. Figure 5.19 shows a longitudinal section (fig. 5.19(a)) and the binary image (fig.5.19 (b)) that represents the segmenting curve. The wavy shape, characteristic of IVUS longitudinal cuts, reflects cardiac motion and is of clinical interest, meanwhile small irregularities are caused by blood turbulence. The model recovered by RCF is a smooth shape (fig.5.19(c)) that keeps the same number of undulations than the original cut.

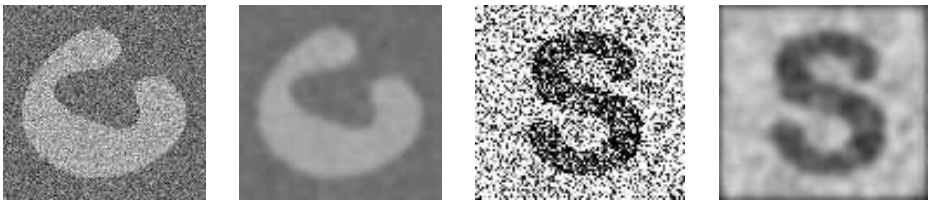

(a) (b) (c) (d)

Figure 5.20: Test Set 1. Noisy images: non convex shape (a), smoothed image (b), character 'S' (c) and smoothed image (d).

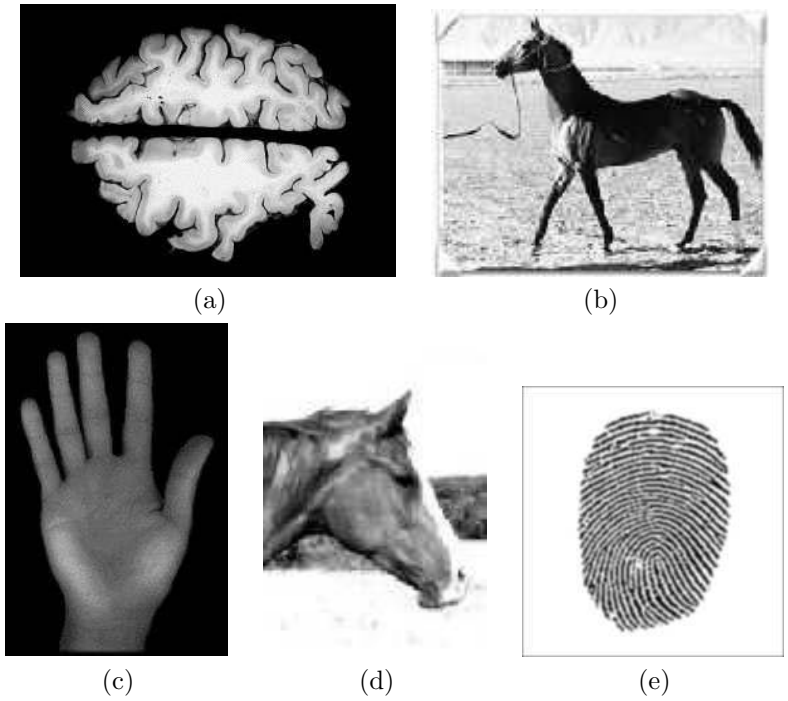

(a) (b)

(c) (d) (e)

Figure 5.21: Test Set 2. Real images: human brain (a), horse (b), hand (c), horse head (d) and fingerprint (e).

5.2 Anisotropic Contour Closing

In this experimental section, we will show the accuracy of the shapes recovered by ACC using dynamic Coherence Vector Fields to guide the restricted extension process. Because we have embedded contour closing in the context of shape restoration oriented to object segmentation, ACC will be applied to contours extracted from real images and synthetic noisy images. Figure 5.20 shows the noisy shapes, a croissant-like curve